Nanoscale

Nanoparticles Speckled by Ready-to-Conjugate Lanthanide Complexes for Multimodal Imaging

Journal:	*Nanoscale*
Manuscript ID:	NR-ART-02-2015-000959.R1
Article Type:	Paper
Date Submitted by the Author:	27-Apr-2015

Complete List of Authors:	Biju, Vasudevan; National Institute of Advanced Industrial Science and Technology, Japan, Health Technology Research Center Hamada, Morihiko; AIST, Health Research Institute Ono, Kenji; Nagoya University, Department of Brain Life Science, Research Institute of Environmental Medicine Sugino, Sakiko; National Institute of Advanced Industrial Science and Technology (AIST), Health Research Institute Ohnishi, Takashi; National Institute of Advanced Industrial Science and Technology (AIST), Health Research Institute Edakkattuparambil, Shibu; IIT Madras, Chemistry Yamamura, Shohei; AIST, Health research institute Sawada, Makoto; Nagoya University, Department of Brain Life Science, Research Institute of Environmental Medicine Nakanishi, Shunsuke; Kagawa University, Department of Advanced Materials Science Shigeri, Yasushi; AIST, AIST Kansai Wakida, S; National Institute of Advanced industrial Science and Technology (AIST), Human Stress Signal Research Center

Nanoscale RSCPublishing

ARTICLE

Nanoparticles Speckled by Ready-to-Conjugate Lanthanide Complexes for Multimodal Imaging

Cite this: DOI: 10.1039/x0xx00000x

Received 00th February 2015, Accepted 00th xxxx 2015

DOI: 10.1039/x0xx00000x

www.rsc.org/

Vasudevanpillai Biju,[a,b,*] Morihiko Hamada,[a,c] Kenji Ono,[d] Sakiko Sugino,[a] Takashi Ohnishi,[a,c] Edakkattuparambil Sidharth Shibu,[a] Shohei Yamamura,[a] Makoto Sawada,[d] Shunsuke Nakanishi,[c] Yasushi Shigeri,[a] Shin-ichi Wakida[a]

Multimodal and multifunctional contrast agents receive enormous attention in the biomedical imaging field. Such contrast agents are routinely prepared by the incorporation of organic molecules and inorganic nanoparticles (NPs) into host materials such as gold NPs, silica NPs, polymer NPs, and liposomes. Despite their non-cytotoxic nature, the large size of these NPs limits the *in vivo* distribution and clearance and inflames complex pharmacokinetics, which hamper the regulatory approval for clinical applications. Here we report a unique method that brings magnetic resonance imaging (MRI) and fluorescence imaging modalities together in nanoscale entities by the simple, direct and stable conjugation of novel biotinylated coordination complexes of gadolinium (III) to CdSe/ZnS quantum dot (QD) and terbium (III) to super paramagnetic iron oxide NP (SPION), but without any host material. Successively, we evaluate the potentials of such lanthanide-speckled fluorescent-magnetic NPs for bioimaging at single-molecule, cell and *in vivo* levels. The simple preparation and small size make such fluorescent-magnetic NPs promising contrast agents for biomedical imaging.

1. Introduction

In vivo multimodal imaging has the potentials to precisely pinpoint the anatomy and physiology associated with the onset and progression of diseases such as cancer. With the infiltration of molecular and nanomaterials contrast agents into the clinical settings, the quality and precision of biomedical imaging technology have significantly reformed in the recent past. Integration of two or even more contrast agents of individual imaging modalities, each complementing the limitation of other agents, into a nanoscale entity is fundamental to multimodal imaging and the extraction of the finest information about pathophysiological conditions. Multimodality in the clinical settings can be readily accomplished by the combination of techniques such as magnetic resonance imaging (MRI), ultrasonography, positron and single photon emission tomography (PET/SPECT), and X-rays-based computed tomography (CT). Nonetheless, some of these techniques pose radiation hazard. Thus, nanomaterials incorporated with contrast agents for fluorescence and magnetic resonance attract much attention for non-invasive *in vivo* multimodal imaging, but without any concern about hazardous radiation.[1-5]

Fluorescent and paramagnetic materials for the construction of multimodal NPs are routinely recruited from among visible/NIR dyes,[6-15] semiconductor quantum dots (QDs),[16-26] upconversion NPs (UCNPs),[27-29] carbon NPs,[30,31] noble metal QCs,[32-35] lanthanide ions,[31,32] SPION,[11-14,24,25,32] oxide[36-39] or vanadate[40,41] of gadolinium, and coordination complexes of lanthanides[6-10,17-22]. Host materials such as NPs of silica,[42] polymers,[43] lipids[44] and carbon[45] have been extensively exploited for accommodating two or more such contrast agents into nanoscale entities through host-guest interactions involving hydrogen bonding,[46] hydrophobicity,[47] π-stacking,[48] nanopore-filling,[49] covalent or coordinate bonding,[50] and stimuli-responsive molecular gates[51]. Additionally, the large surface area, unique pores, and versatile chemistry of the host materials allow one for recruiting drugs/genes, molecules such as antibodies and peptides for targeted labelling, and certain stimuli for the release/delivery of contrast agents or drugs/genes.[52,53] Nonetheless, the large size of the final product, which is largely contributed by the host material, poses a major challenge in both their distribution to the parenchymal target organ/lesion and clearance from the body. Therefore, simple and small-size multimodal contrast agents are constantly sought-after towards practical applications in the clinical settings by the direct doping, co-precipitation, adsorption, or non-covalent or covalent conjugation of a fluorophore to a paramagnetic agent or *vice versa*.

The covalent conjugation offers stability to multimodal contrast agent when compared with those prepared by doping, co-precipitation, or adsorption. For example, stable contrast agents for MRI and fluorescence imaging are prepared by the conjugation of Gd(III) complexes to organic dyes such as porphyrin,[6,7] fluorescein[8] and Cy5.5,[9,10] QDs such as $CuInS_2/ZnS$,[17,18] silicon,[19] InP,[20] CdSeTe/CdS,[21] CdSe/ZnS[22] and CdTe/ZnS,[23] persistent luminescence NPs,[54] UCNP,[27-29] and gold QCs.[32-35] Similarly, fluorescent-magnetic bimodal NPs prepared by the conjugates of dye molecules such as Cy5.5,[11] rhodamine,[12,13] Congo red[13] and Eu (III) complex,[14] QDs such as CdSe/ZnS[24] and CdTe,[25] and Au QCs[32] to SPION have been found attractive for the combined MRI and fluorescence imaging. Gd(III) complexes employed in multimodal NPs are prepared using ligands such as 1,4,7,10-tetraazacyclododecane-1,4,7,10-tetraacetic acid (DOTA) or diethyltriamine pentaacetic acid (DTPA) functionalized with N-hydroxysuccinimide (NHS) or biotin for the successive conjugation to amine or streptavidin functionalized fluorophores. Although the synthesis of such ligands are doable in a typical organic chemistry laboratory, simple and cost-effective preparation of ready-to-conjugate complexes of lanthanides such as Gd (III), Eu (III) and Tb (III) is highly desirable for biomedical applications. Here we report simple and small-size fluorescent-magnetic bimodal NPs prepared by the direct conjugation of novel biotinylated DOTA-Gd(III) complexes to streptavidin-functionalized CdSe/ZnS QDs and biotinylated DOTA-Tb(III) complexes to streptavidin-functionalized SPION, but without any sophisticated chemical reaction or host material. A simple biotinylated-DOTA derivative prepared by the direct condensation between one of the carboxylic acid groups in DOTA and ω-bromopropyl ester of biotin is utilized in the preparation of the complexes and the fluorescent-magnetic NPs. Successively, these NPs were conjugated by epidermal growth factor (EGF), and the potentials of the EGF-conjugated NPs for single-molecules, cells and *in vivo* imaging were evaluated in human lung epithelial adenocarcinoma (H1650) cells or B6 mice.

3. Results and Discussion

Two types of novel fluorescent-magnetic NPs prepared by the direct tethering of coordination complexes of biotinylated Gd(III)-DOTA complexes to streptavidin functionalized CdSe/ZnS QDs and biotinylated Tb(III)-DOTA complexes to SPION enabled us for obtaining the combined MRI and fluorescence images *in vitro* and i*n vivo*. The biotinylated complexes are prepared by the simple chemical reactions shown in Fig. 1. At first, a ω-bromopropyl ester of biotin (**2**), which was prepared by the 1,8-diazabicyclo[5.4.0]undec-7-ene (DBU)-catalyzed reaction between 1,3-dibromopropane and biotin, was conjugated to one of the carboxylic groups of 1,4,7,10-tetraazacyclododecane 1,4,7,10-tetraacetic acid (DOTA) to provide the biotinylated ligand **3**. Successively, biotinylated Gd (III)-DOTA complex (**4**) was prepared by the reaction of **3** with $GdCl_3$. Similarly, biotinylated Tb(III)-DOTA complex (**5**) was prepared using $TbCl_3.6H_2O$. The complexes were prepared by a procedure similar to that reported by Brittain and Desreux.[55] We followed the formation of **5** by recording the absorption and fluorescence spectra (Fig. 2A) of the reaction mixture at different time intervals. Also, MALDI-TOF mass spectra was employed in the characterization of the complex. The characteristic fluorescence band of Tb(III) complex with the main band ca 545 nm, which is due to the 5D4→7F5 transition in Tb (III)[56,57] was helpful for the detection of **5**. Further, we confirmed the formation of **5** from an increase and saturation in the fluorescence intensity (Inset of Fig. 2A) of **5** with time under reaction, which is due to the replacement of water ligands of Tb (III) by oxygen (COOH groups) and nitrogen (cyclen ring) atoms of **3** and the associated absorption-energy transfer-emission (AETE) mechanism.[57] On the other hand, the fluorescence intensity of an aqueous solution of Tb (III) ions, but without **3**, remained intact upon heating. These results confirm the formation of **4** and **5**. Details of preparation and characterization of **2-5** are provided in the experimental section. The fluorescent-magnetic NPs, **6** and **7**, were prepared by the direct tethering of **4** and **5** to the biotin-binding sites of streptavidin moieties on QD and SPION, respectively (Fig. 1). Fig. 2B and C shows the TEM images of **6** and **7**.

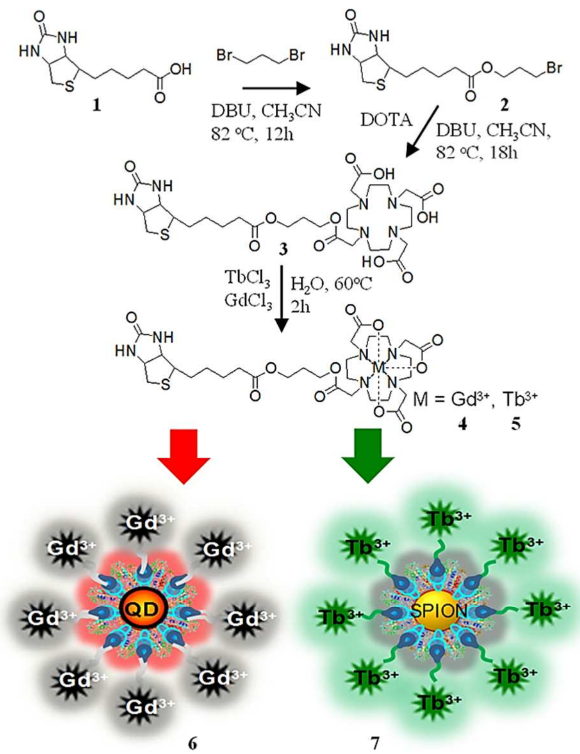

Fig. 1. Preparation of biotinylated DOTA (**3**) and ready-to-bioconjugate complexes of Gd(III) (**4**) and Tb(III) (**5**), and illustration of lanthanide-speckled fluorescent-magnetic NPs (**6** and **7**) prepared by the conjugation of biotinylated Gd(III)-DOTA to streptavidin-functionalized CdSe/ZnS QDs or biotinylated Tb(III)-DOTA to streptavidin-functionalized SPION.

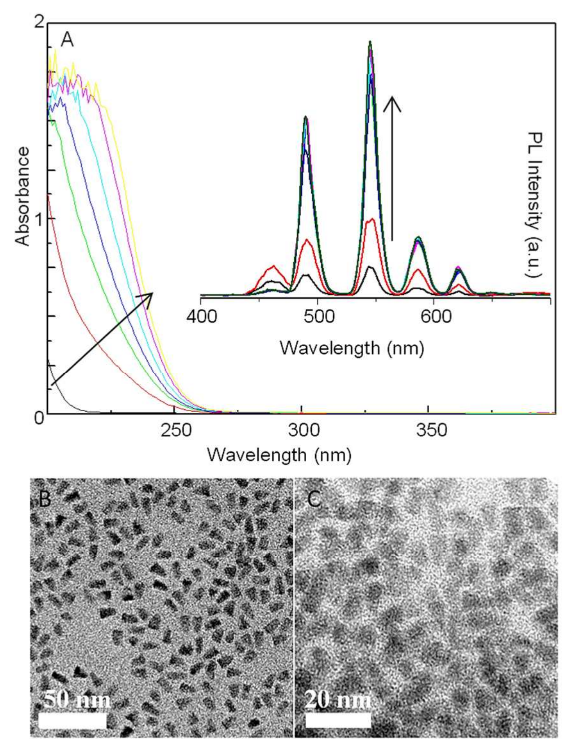

Fig. 2. (A) Absorption and (inset) fluorescence spectra of 260 nM aqueous solution of **5** recorded at 20 min intervals under continuous heating during the preparation of the complex. (B,C) TEM images of **6** (B) and **7** (C). The wavelength of excitation light was 230 nm in A.

To evaluate whether or not the conjugation of **4** to QDs affects the properties of QDs, we recorded and analyzed the steady-state absorption (traces a-d in Fig. 3A) and photoluminescence (PL, traces a'-d' in Fig. 3A) spectra and the nanosecond PL decay profiles (inset of Fig. 3A) of QD655 and QD705 before and after the conjugation of **4**. As seen in Fig.3A, the absorbencies of QDs (QD655 or QD705) are not affected by **4**. The slight difference in the optical density (<300 nm) of **6** when compared with that of pristine QD is attributed to the absorption of UV light by **4**. Further, the changes in the PL quantum efficiencies [Φ_f = 79% for QD655 and Φ_f = 51% for QD705] and PL lifetimes (τ_{PL} = 12 ns for QD655 and τ_{PL} = 41 ns for QD705) of QDs after conjugation of **4** were negligible. Here, the Φ_f values of QDs were provided by the manufacturer; whereas, the PL lifetime values were experimentally determined by fitting the PL decay profiles to the third order kinetics. We assume that the spatial separation between the complex and the QD, which is provided by the polymer and streptavidin coating on QD, preserves the physical properties of the QD core in **6**. These observations suggest that stable multimodal NPs can be routinely constructed by the direct tethering of ready-to-conjugate lanthanide complexes to NPs such as QDs and SPIONs, but without considerably affecting the size or properties of the NPs.

Lanthanide-speckled fluorescent-magnetic NPs for cell labeling and *in vivo* applications were prepared by the recruitment of 1

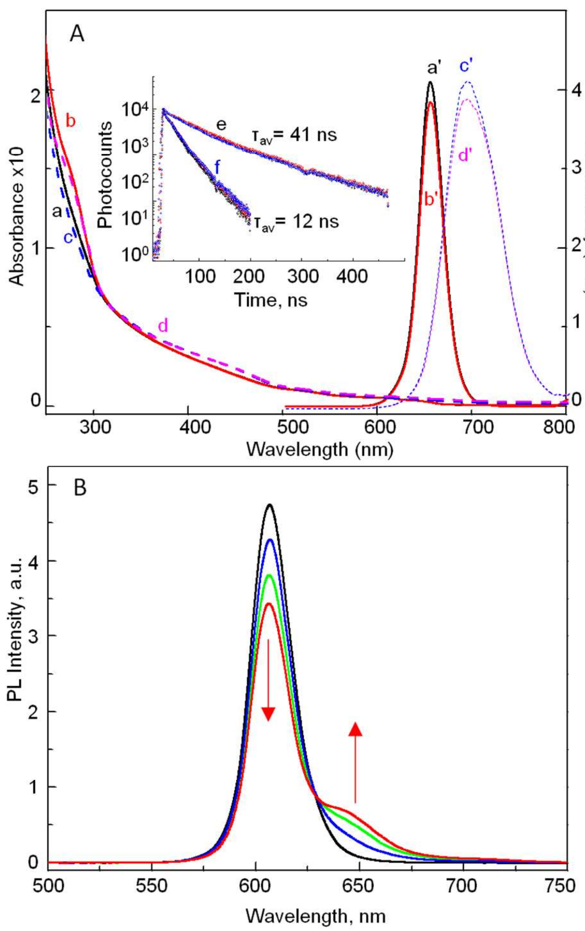

Fig. 3. (Aa-d) Absorption and (Aa'-d') PL spectra of aqueous solutions of (a,a',c,c') CdSe/ZnS QDs and (b,b',d,d') **6** with Emλ_{max} at (a,a',b,b') 655 and (c,c',d,d') 705 nm. (B) Fluorescence spectra of a 20 nM QD605-streptavidin solution recoded without and with different concentrations (10, 20, and 30 nM) of biotin-EGF-AlexaFluor633 conjugate. The shoulder band at ca 640 nm indicates the avidin-biotin conjugate formation and the successive FRET from QD to AlexaFluor633. The wavelength of excitation light is 400 nm.

equivalent of biotinylated EGF ligand to the surface of QD or SPION, which was prior to the tethering of multiple coordination complexes (**4** or **5**). Here, EGF is selected by considering the over-expression of EGF receptors (EGFR) in the cell line used, which is human lung epithelial adenocarcinoma cells (H1650). At first, human recombinant EGF was biotinylated using biotin sulfo-NHS ester, and purified by gel-filtration on a Sephadex G25 column. The biotinylated EGF molecules were tethered (at 1:1 EGF-biotin:QD/SPION) to streptavidin on QD/SPION over 30 min at room temperature, which was followed by the conjugation of **4** to QD and **5** to SPION at 10:1 equivalences (**4**:QD and **5**:SPION).

The binding of biotinylated EGF molecules to streptavidin on the NPs was tested by Förster resonance energy transfer (FRET) measurements. Here, a FRET system was constructed using CdSe/ZnS QD as the energy donor and AlexaFluor633 as the acceptor. At first, AlexaFluor633-labeled EGF was prepared by the reaction between biotinylated EGF (50 µL, 6 µM) and NHS ester of AlexaFluor633 (50 mL, 30 µM) over 1h at room temperature. The labeled EGF molecules were purified by repeated (3 times) dialysis against a membrane for 2kDa, during which low molecular mass compounds such free AlexaFluor633 NHS ester were eliminated. The binding of biotinylated EGF-AlexaFluor633 conjugate to streptavidin-QD conjugate (Emλ_{max} = 605 nm) was analyzed by obtaining the fluorescence spectra of mixtures of the two at different concentrations. As the concentration of EGF-AlexaFluor633 was increased in the mixture, the PL intensity of QDs (energy donor) was decreased, which was associated with the appearance and enhancement of the characteristic fluorescence band of AlexaFluor633 (Fig. 3B). These results suggest FRET from QD to AlexaFluor633, which is due to the binding of biotinylated EGF to streptavidin on QDs.

The potential of EGF-conjugated fluorescent-magnetic NPs for bioimaging *in vitro* is tested in H1650 cells. The cells cultured up to 70% confluence were washed with phosphate buffered saline (PBS) and treated with 1 nM solutions of EGF-QD, EGF-**6** or EGF-**7** conjugate for 1h at ice-cold conditions. During this step, the cells were labeled by the conjugate, which is due to the specific binding of EGF ligands to EGFR molecules over-expressed in the plasma membrane of H1650 cells. The labeled cells were copiously washed with PBS, harvested using trypsin, and made into pellets for MRI and fluorescence imaging. We selected cell pellets instead of single cells because of the technical challenge associated with MRI of single cells. MRI of cell pellets labeled with biomarker-specific contrast agents has been exploited in the characterization of biomolecules,[58] tumor cells,[59,60] and apoptosis.[61] Fig. 4A-E shows the fluorescence image and MRI of QDs, SPION, **4-7**, and H1650 cell pellets with or without labeling using EGF-**6** or EGF-**7**. The NIR (705 nm) PL of QDs, (Figs. 3A and 4B), and the enhancement of T1- and T2-weighted MRI contrasts of cells labeled with EGF-**6** show the potentials of NIR QD specked by Gd(III) complex for multimodal bioimaging. The bright MRI contrast of labeled cells (Fig. 4Cb), when compared with cells that are not labeled (Fig. 4Cc) and solutions of **4** (Fig. 4Cd) and **6** (Fig. 4Ca) is attributed to the changes in the magnetic relaxation of the protic organelles such as EGFR and endosomes of labeled cells. Nonetheless, the T1-weighted contrasts of **4** and **6** in the solution phase are comparable to that of a QD solution (Fig. 4Ce) or the buffer (Fig. 4Dh). The poor contrast of samples when compared with the labeled cells is attributed to the free diffusion of molecules or NPs in the solution phase. Enhancement in the T1-weighted MRI contrast was also observed for cells labeled with EGF-**7**. As SPION-based particles are ideal T2-contrast agents,[11-14,24,25,32]

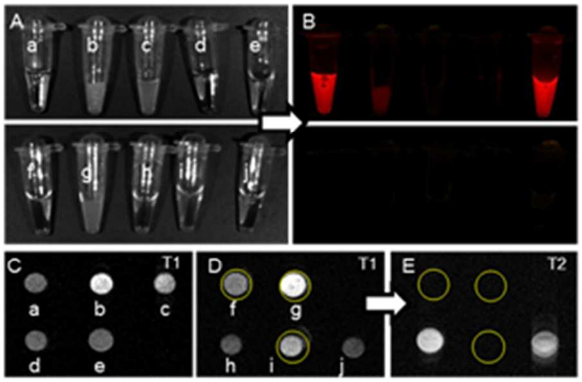

Fig. 4. (A) Bright filed images, (B) fluorescence images and (C-E) MRI of sample solutions and H1650 cell pellets: (a) **6**, (b) cells labeled with **6**, (c) unlabeled cells, (d) **4**, (e) QD705, (f) **7**, (g) cells labeled with **7**, (h) PBS, (i) SPION and (j) **5**.

we have recorded and analyzed the T2-weighted MRI of sample solutions (**5**, SPION, and **7**) and H1650 cells labeled with EGF-**7**. Interestingly, an enormous increase in the MRI (T2) contrast (darkening) of labeled cells [Fig. 4Dg (T1) to Fig. 4E (T2)] was observed, which is comparable to the darkening of T2-weighted MRI contrasts of a solution of SPION [Fig. 4Di (T1) to Fig. 4E (T2)]. Nevertheless, the absorption band in the UV region (Fig. 3A) and prominent fluorescence bands in the blue-green regions of **5** are major limitations of **7** for fluorescence-based bioimaging. Thus, we focus our further studies on EGF-**6**, where the properties of QDs such as exceptional brightness and photostability, broad absorption of light in the Vis-NIR region, large Stokes shift and NIR PL (655 or 705 nm) are combined with the MRI contrast of Gd(III) complex for bioimaging.

Fluorescence microscopy was employed in the single-molecule detection of EGF-**6** conjugate in living cells. Here, H1650 cells cultured up to 70% confluence in 60 mm tissue culture plates were labeled using a 1 nM solution of EGF-**6** or EGF-QD conjugate. The labeling was carried out at ice-cold conditions, which minimizes the endocytosis of the conjugate during the labeling step. Further, the nuclei of the cells were stained with Syto21 or Syto13 dye by following the methods reported in the literature.[24,32] The labeled cells were copiously washed with PBS, the medium was changed to Dulbecco's Modified Eagles Medium (DMEM), excited with 400 nm (for Syto dyes) or 532 nm (for QDs) laser beam, and observed in an inverted optical microscope. Fluorescence image of the cells labeled using EGF-**6** conjugate (Fig. 5A) indicates efficient intracellular delivery of the conjugate, which is comparable to the endocytosis of EGF-QD conjugate (Fig. 5B, C). On the other hand, control cells incubated with **6** or QD, but without any EGF do not show any intracellular fluorescence. The intracellular delivery of the conjugate takes place by binding to EGFR, which is over-expressed in the plasma membrane of H1650 cells, and subsequently, the EGFR-EGF-**6** assembly is engulfed by receptor-mediated endocytosis.

To analyse the binding of EGF to EGFR and the subsequent intracellular pathway of EGF-**6**/EGF-QD conjugates, H1650 cells were labeled with simple EGF-QD conjugate and the time- and intensity- gated single-molecule fluorescence of EGF-EGFR complexes were recorded. Here, EGFR in the plasma membrane of H1650 cell was activated by applying a solution (1 nM) of EGF-QD conjugate. As seen in Fig. 5C, immediately (<15 min) after the activation, EGF-EGFR complexes were present

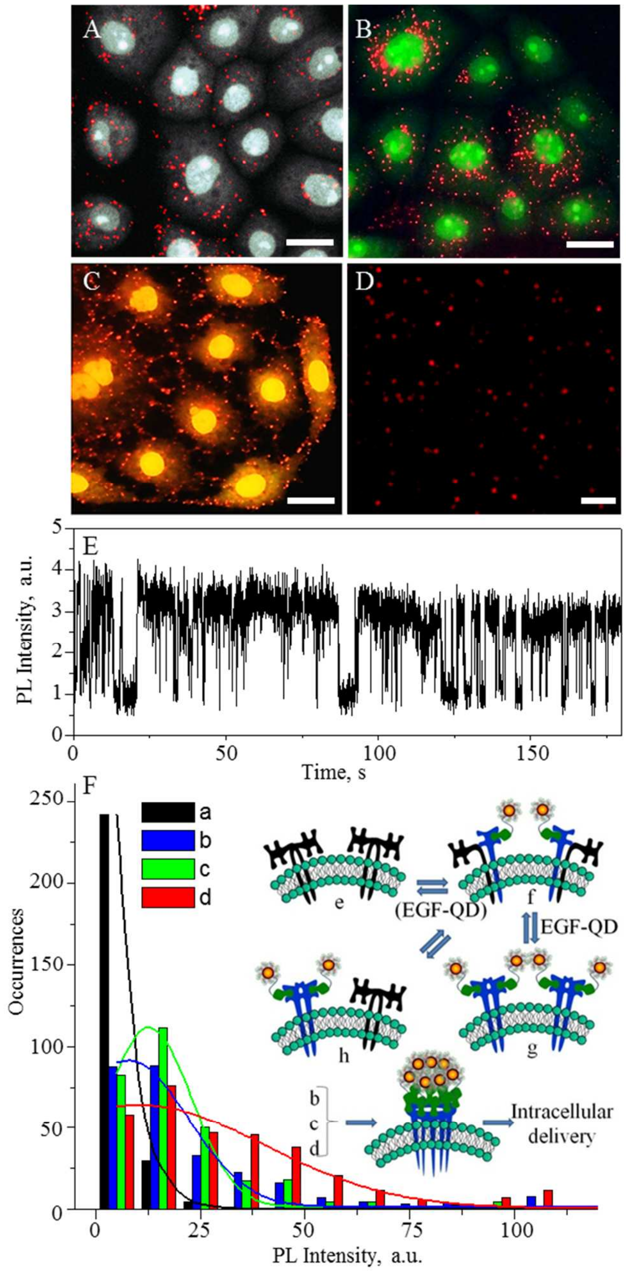

Fig. 5. PL images and intensity distributions of EGFR single-molecules in H1650 cells: (A) cells labeled with EGF-**6** and (B,C) cells labeled with EGF-QD conjugates. The nuclei in A and B are stained with Syto13 dye and that in C with Syto 21 dye. (D) Fluorescence image of single QDs tethered on a glass substrate and immersed in water. (E) PL intensity trajectory of a single QD in D. QDs were excited with 532 nm laser beam and Syto dyes with 400 nm laser beam. The fluorescence of Syto 13, Syto21 and QDs are collected through band-pass or long-pass filters. (F) PL intensity histograms of (a) single QDs attached on a glass substrate and (b-d) EGFR in H1650 cells activated with EGF-QD conjugates and recorded at (b) ca 15 min, (c) ca 30 min and (d) >1h after the labeling. Inset of F: presentation of the labeling, dimerization and clustering of EGFR in cells activated with EGF-**6** or EGF-QD conjugates. Scale bars: (A-C)-20 μm, (D) 10 μm.

preferentially in the cell membrane, mostly attached to the filopodia or lamellipodia. The blinking and PL intensities of individual fluorescence spots in the cell membrane were

comparable to that of pristine QDs tethered on a glass substrate (Fig.5D, E), validating the detection of EGFR single-molecules.Fig. 5F shows PL intensity histograms of fluorescence spots detected at different time intervals after the activation of EGFR with EFG-QD conjugate. Interestingly, a uniform distribution of EGFR molecules, with fluorescence intensities equivalent to 1 or 2 QDs, was detected immediately (<15 min) after the activation (Fig. 5Fb). However, brighter fluorescence spots were emerged with time under incubation. Temporal changes in the intensities of fluorescence spots, which are assigned to the dimerization and clustering of receptors,[62] was examined by the correlation of the time- and intensity- gated fluorescence images of >500 single molecule receptors in the cell membrane with that of QDs tethered on a glass substrate. Within 15 min of post activation of EGFR, majority (>80%) of the receptors were bound with one or two EGF-QD conjugates (Fig. 5Fb). During the next 15 to 30 min, the occurrences equivalent to dimers and larger clusters were increased. As a result of this increase, the histogram shifted to the higher intensity side (Fig. 5Fc,d). The fluorescence spots with intensity equivalent to that of a single QD are attributed heterodimers of EGFR, i.e. EGFR pre-dimers (Fig. 5Fe) ligated by only one EGF-QD conjugate (Fig. 5Ff). An increase in the number of fluorescence spots with intensity equivalent that of two QDs suggests the formation of signaling dimers (Fig. 5Fg and h) as a result of either the activation of each pre-dimer by two EGF-QD conjugates (Fig. 5Fg) or association and disproportionation of two heterodimers (Fig. 5Ff) into a signaling dimer and a pre-dimer,[62] which is indicated in Fig. 5Ff-h. The high intensity fluorescence spots, which dominated with time under incubation, suggest clustering of dimers.[62,63] The larger clusters are eventually transported into the cytoplasm and subsequently accumulated in the perinuclear lysosome organizing region (Fig. 5A,B). These results suggest that EGF-QD and EGF-**6** conjugates allow us for detecting and following single-molecules, dimers and clusters of EGFR in living cells.

Despite the unique optical and magnetic properties of nanomaterials, toxicity is an unsolved central issue that hampers their biological applications.[64-68] Toxicity of nanomaterials can be size-, surface- or materials- related. Therefore, a general solution to the toxicity of nanomaterials is far from reality, and case-by-case analysis is often necessary. We examined the cytotoxicity of EGF-**6** conjugate by the assay of mitochondrial reductase enzyme activity (MTT assay) in H1650 cells labeled with the conjugate and compared the results with that of unlabeled cells and cells labeled with EGF-QD conjugates. The viability of cells is retained above 90% (Fig. 6A) when treated with EGF-**6** solutions having concentrations up to 10 nM, which is an order of magnitude higher than that employed in cell labeling and imaging (Fig. 5A). As seen in Fig. 6A and B, the viability of cells labeled with EGF-**6** conjugate is comparable or marginally higher than that of those labeled with EGF-QD conjugates. These observations not only confirm the biocompatibility of **6** but also suggest multiple Gd(III) complexes on QDs do not induce any cytotoxic effect to QDs .

Despite the *in vitro* non-cytotoxic nature, when applied *in vivo,* most nanomaterials interact with the reticuloendothelial systems and inflame complex pharmacokinetics, hampering regulatory approval for clinical applications. In other words, uniform biodistribution and efficient renal or hepatobiliary excretion are fundamental prerequisites for *in vivo* applications of nanomaterials- from biomedical imaging to drug delivery and

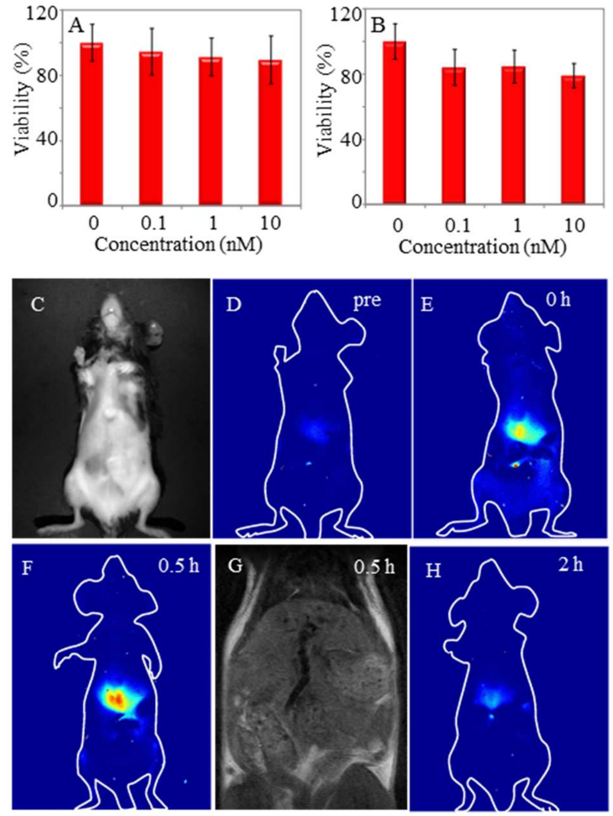

Fig. 6. Cytotoxicity assay and *in vivo* imaging. (A, B) Histograms of MTT assays for H1650 cells labeled with different concentrations of (A) 6-EGF and (B) QD-EGF conjugates. (C-H) Images of a B6 mouse: (C) bright-field optical and (D) fluorescence images recoded before injection of EGF-**6** conjugate, (E-H) fluorescence images and MRI recorded after the intravenous injection of a 20 nM solution of EGF-**6** conjugate: (E) fluorescence image acquired immediately after the injection, (F) fluorescence image acquired at ca 30 min post injection, (G) T1-weighted MRI acquired at ca 30 min post injection, and (H) fluorescence image acquired at ca 2 h post injection.

cancer therapy. We evaluated the potentials of lanthanide-speckled fluorescent-magnetic NPs for *in vivo* imaging in B6 mice, and observed the *in vivo* fate of the NPs. Here a 20 nM solutions of EGF-6 conjugate was administrated in nude mice by the intravenous injection. The MRI and fluorescence images of the mice were acquired before and at different time intervals after the injection. Within 30 min post injection, (Fig. 6E, F), the NPs were mostly accumulated in the liver. Also, an increase in the MRI contrast of the liver was detected in the T1-weighted image (Fig. 6G). The PL fluorescence from the liver was diminished over 2 h (Fig. 6H) and touched the background level within 24 h post injection. These results show not only the efficient detection of the NPs from deep tissues such as the liver but also the clearance of the NPs. The decrease and disappearance of PL can be assigned to excretion through the renal pathway, which was heretofore observed for QDs[69] and QD-based fluorescent-magnetic NPs.[24] Yet, we do not rule out a possibility that the NPs were degraded by the liver enzymes. While we focus the current studies on the preparation of novel lanthanide-speckled NPs for multimodal imaging, long-term pharmacokinetics and toxicity of such NPs need further attention.

Conclusions

We demonstrate the preparation of simple fluorescent-magnetic NP

contrast agents by the direct conjugation of novel ready-to-bioconjugate complexes of Gd(III) or Tb(III) to the surface of QDs or SPION. Further, by the recruitment of EGF hormone to the surface, these NPs were efficiently delivered in human lung epithelial adenocarcinoma cells in which EGFR is over-expressed. The potentials of the lanthanide-speckled NPs composed of QDs/SPION and ready-to-bioconjugate coordination complexes Gd(III)/Tb(III) for bioimaging are realized by obtaining MRI and fluorescence images of sample solutions, EGFR single-molecules, live cells and mice. The straightforward preparation, T1- and T2-weighted MRI contrast, bright and stable NIR fluorescence, and biocompatibility make NPs decorated with multiple coordination complexes promising for biomedical imaging and image-guided therapy.

2. Experimental Section

2.1. Materials

All the chemicals and solvents used in the preparation, purification and characterization of the complexes and fluorescent-magnetic NPs were analytical grade. Streptavidin-functionalized CdSe/ZnS QD samples ($Em\lambda_{max}$ =605/655/705 nm) and AlexaFluor633-NHS ester were obtained from Life Technologies and SPION was from NANOCS. Biotin and DOTA were obtained from Wako Chemicals, lanthanide salts and DBU were from Sigma-Aldrich, and 1,3-dibromopropane was from Tokyo Chemical Industries.

Steps involved in the preparation of biotinylated Gd(III) and Tb(III) complexes and the lanthanide speckled fluorescent-magnetic NPs are summarized in Fig. 1. First, ω-bromopropyl ester of biotin (**2**) was prepared by the reaction between biotin (1 g, 4.09 mmol) and 1,3-dibromopropane (2.42 g, 12.0 mmol), which was catalyzed by DBU (980 µL, 6.55 mmol). Here, biotin was dissolved in acetonitrile (25 mL) by the addition of DBU, which was followed by the addition of 1,3-dibromopropane. This reaction mixture was heated at 82 ° for 12 h with vigorous stirring. Successively, the reaction mixture was cooled at room temperature, during which a light white precipitate was formed. The amount of the precipitate was increased with the drop-wise addition of *n*-hexane (less than 4 mL) to the crude reaction mixture. The white precipitate was collected by filtration through a Whatman grade 1 filter paper, re-dissolved in chloroform and purified by column chromatography on silica gel (200-400 mesh) using dichloromethane as the eluent to yield **2** in 80 %. ^1H NMR (400 MHz, $CDCl_3$): ∂ = 1. 46 (m, 2H), 1.70 (m, 4H), 2.18 (m, 2H), 2.35 (t, 2H), 2.74 (m, 1H), 2.94 (m, 1H), 3.16 (m, 1H), 3.47 (t, 2H), 4.21 (t, 2H), 4.34 (m, 1H), 4.56 (m, 1H), 5.16 (s, 1H), 5.56 (s, 1H); ^{13}C NMR (100 MHz, $CDCl_3$): ∂ = 29, 32.5, 34, 36, 38, 45, 53, 59, 64.5, 66.5, 101, 167, 178; MALDI-TOF ($C_{13}H_{21}N_2O_3BrS$) m/z = 365.

Biotinylated DOTA (**3**) was prepared by the DBU-catalyzed condensation between one of the carboxylic groups of DOTA and the ω-bromo group of **2**. In this condensation reaction, a mixture of DOTA (200 mg, 0.495 mmol), **2** (200 mg, 0.619 mmol) and DBU (300 µL, 2.01 mmol) was dissolved in acetonitrile (50 mL) and stirred at 82 °C for 18 h (Fig. 1). Here, the amount of DBU was set at 300 mL for the complete solubilization of DOTA. After 18h, the reaction mixture was cooled by placing first at room temperature and then in an ice bath. Upon addition of a dilute solution of trifluoroacetic acid (300 µL in 10 mL dichloromethane), the crude product was separated into an off-white heavy liquid in the ice-cold reaction mixture. After the supernatant was decanted, the crude product was dissolved in 5 mL methanol. Successively, upon addition of

15 mL acetone, **3** was collected as a white precipitate, which was
further purified by the repeated precipitation from methanol:acetone mixture (1:4) to provide **3** in 65% yield. ^1H NMR (400 MHz, CD_3OD): ∂ = 1.32 (m, 2H), 1.45 (m, 4H), 1.86 (m, 2H), 2.20 (t, 2H), 2.60 (ds, 1H), 2.82 (dd, 1H), 3.38 (bs, 6H), 3.76 (bs, 16H), 3.89 (bs, 2H), 4.07 (t, 2H), 4.13 (t, 2H), 4.22 (q, 1H), 4.40 (q, 1H); ^{13}C NMR (100 MHz, CD_3OD): ∂ =23.01, 24.77, 27.90, 28.33, 28.54, 33.57, 39.85, 48.89, 49.92, 50.95, 51.09, 52.98, 53.19, 54.13, 55.04, 55.87, 60.45, 60.83, 61.86, 62.24, 115.57, 118.49, 161.55, 161.89, 164.91, 168.98, 170.75, 172.43, 174.22; MALDI-TOF ($C_{29}H_{48}N_6O_{11}S$) m/z = 689. Ready-to-bioconjugate complexes of Gd(III) and Tb(III) were prepared by the reactions of $GdCl_3$ or $TbCl_3.6H_2O$ with **3**. We followed a literature method for the preparation of DOTA complexes.[55] At first, aqueous solutions (1 mL each) of **3** (4.1 mg, 5.95 µmol) and $GdCl_3$ (36.9 mg, 140 µmol) were prepared and the pH of the solutions was adjusted to 8 by the addition of dil. (10 mM) NaOH solution. Next, these two solutions were mixed and heated at 60 °C for 2 h to obtain **4**. Similarly, **5** was prepared from a mixture of solutions of **3** (1 mg, 1.45 µmol) and $TbCl_3$ (2 mg, 5.36 µmol), each in 1 mL water. We employed absorption, fluorescence and MALDI-TOF mass spectroscopy in the characterization of these complexes. **4**: m/z (845.8) and **5**: m/z (846.4).

2.2. Methods

^1H and ^{13}C NMR spectra were acquired in a JEOL 400 MHz spectrometer and MALDI/LDI-TOF mass spectra were recorded in a BRUKER Microflex spectrometer. Fluorescence images of labeled H1650 cells were acquired in an inverted optical microscope (Olympus IX70) equipped with a 40x objective lens, long-pass or band-pass filters for Syto dyes and QDs, and an iXon3 EMCCD (Andor Technology) or a digital CCD camera (Olympus). The excitation light used was either 400 nm femtowave (details are provided below) for Syto dyes or 532 nm cw laser (Millennia II, Spectra Physics) for QDs. Intensities of fluorescence spots were obtained by analyzing the PL intensity trajectories of single-molecule videos recorded using the EMCCD camera. Details of single-molecule measurements are reported elsewhere.[70-73] Fluorescence images and MRI of sample solutions, cell pellets and mice were acquired using a small animal imaging system (Maestero, Perkin-Elmer) and a MRI machine (MR Technology, Inc., Japan). Fluorescence images of samples, cell pellets and mice were analyzed using the Maestro or Image-Pro Plus software (Roper Industries, Inc., USA).

Steady-state fluorescence/PL spectra were recorded using a fluorescence spectrophotometer (Hitachi FL4500). PL decay profiles were recorded using an assembly of a polychromator (Chromex-250IS) and a streak-scope (Hamamatsu-C4334). Details of PL lifetime measurements are reported elsewhere.[72-75] The samples were excited using 400 nm pulses generated from the SHG crystal of an optical parametric amplifier (Coherent OPA 9400) and the fluorescence signals collected through suitable band-pass or long-pass filters were focused at the entrance slit of the polychromator and recorded using the streak-camera.

Cytotoxicity Assay: Cytotoxicity of NPs was evaluated by MTT assay (MTT cell proliferation kit, Roche Diagnostics). Here, ca. 1 million H1650 cells/plate were inoculated into 96-well tissue culture plates (FALCON) containing DMEM supplemented with 10% FBS, and cultured at 37^{o}C for 48 h. After the cells were copiously washed with PBS, the medium was exchanged with DMEM (without FBS) supplemented with different concentrations (0.1 to 10 nM) of EGF-QD or EGF-**6**

conjugate. After 1 h incubation, the cells were copiously washed
with PBS and supplemented with MTT solution (10 μL/well, 5 mg/mL) and DMEM-FBS medium. After 4 h incubation at 37 ^{o}C, the cells were lysed using the lysis buffer (100 μL/well), which is 10% sodium dodecyl sulfate in 0.01 M HCl. The intracellular formazan crystals formed from MTT, which was the result of the metabolic activity of mitochondrial reductase enzyme, were dissolved overnight at 37 ^{o}C. The viabilities of unlabeled cells and those labeled with EGF-QD or EGF-**6** were determined by the measurement of the absorbance of formazan at 550 nm.

Acknowledgements

This work was carried out under the Precursory Research for Embryonic Science and Technology (PRESTO) program of Japan Science and Technology Agency (JST). Also, this work was supported by the Japan Society for the Promotion of Science under the Kaken-hi Grant 24750029. We thank Ayami Nishioka of Kagawa University for TEM experiments.

Notes and references

[a]Health Research Institute, National Institute of Advanced Industrial Science and Technology (AIST), 2217-14 Hayashi-Cho, Takamatsu, Kagawa 761-0395, Japan ; E-mail: v.biju@aist.go.jp
[b]Precursory Research for Embryonic Science and Technology (PRESTO), Japan Science and Technology Agency, Tokyo, Japan
[c]Department of Advanced Materials Science, Kagawa University, 2217-20, Takamatsu, Kagawa 761-0395, Japan
[d]Research Institute of Environmental Medicine, Nagoya University, Nagoya 464-8601, Japan
VB and MH contributed equally to the experiments

1. J. Cheon, J. H. Lee, *Acc. Chem. Res.* 2008, **41**, 1630.
2. J. Kim, Y. Piao, T. Hyeon, *Chem. Soc. Rev.* 2009, **38**, 372.
3. A. Y. Louie, *Chem. Rev.* 2010, **110**, 3146.
4. M. Mahmoudi, V. Serpooshan, S. Laurent, *Nanoscale* 2011, **3**, 3007.
5. D. E. Lee, H. Koo, I. C. Sun, J. H. Ryu, K. Kim, I. C. Kwon, *Chem. Soc. Rev.* 2012, **41**, 2656.
6. X. S. Ke, J. Tang, Z. S. Yang, J. L. Zhang, *J. Porph. Phthalocyan.* 2014, **18**, 950.
7. A. Eggenspiller, C. Michelin, N. Desbois, P. Richard, J.-M. Barbe, F. Denat, C. Licona, C. Gaiddon, A. Sayeh, P. Choquet, C. P. Gros. *Eur. J. Org. Chem.* 2013, 6629.
8. V. S. R. Harrison, C. E. Carney, K. W. Macrenaris, T. J. Meade, *Chem. Commun.* 2014, **50**, 11469.
9. M. Liang, X. Liu, D. Cheng, G. Liu, S. Dou, Y. Wang, M. Rusckowski, D. J. Hnatowich, *Bioconjugate Chem.* 2010, **21**, 1385.
10. T. Nam, S. Park, S. Y. Lee, K. Park, K. Choi, I. C. Song, M. H. Han, J. J. Leary, S. A. Yuk, I. C. Kwon, K. Kim, S. Y. Jeong, *Bioconjugate Chem.* 2010, **21**, 578.
11. H. Arami, A. P. Khandhar, A. Tomitaka, E. Yu, P. W. Goodwill, S. M. Conolly, K. M. Krishnan, *Biomaterials*, 2015, **52**, 251.
12. T. T. Sibov, L. F. Pavon, L. A. Miyaki, J. B. Mamani, L. P. Nucci, L. T. Alvarim, P. H. Silveira, L. C. Marti, L. F. Gamarra, *Int. J. Nanomed.* 2014, **9**, 337.
13. H. Skaat, S. Margel, *Biochem. Biophys. Res. Commun.* 2009, **386**, 645.
14. J. Liu, W. Zhang, H. Zhang, Z. Yang, T. Li, B. Wang, X. Huo, R. Wang, H. Chen, *Chem. Commun.* 2013, **49**, 4938.
15. S. K. Yen, D. Janczewski, J. L. Lakshmi, S. Bin Dolmanan, S. Tripathy, V. H. B. Ho, V. Vijayaragavan, A. Hariharan, P. Padmanabhan, K. K. Bhakoo, *et al., ACS Nano* 2013, **7**, 6796.
16. L. Jing, K. Ging, S. V. Kershaw, I. M. Kempson, A. L. Rogach, M. Gao, *Adv. Mater.* 2014, **26**, 6367.
17. B. Lin, X. Yao, Y. Zhu, J. Shen, X. Yanga, C. Lia, *RSC Adv.* 2014, **4**, 20641.
18. C.-Y. Cheng, K.-L. Ou, W.-T. Huang, J.-K. Chen, J.-Y. Chang, C.-H. Yang, *ACS Appl. Mater. Interf.* 2013, **5**, 4389.
19. F. Erogbogbo, C. W. Chang, J. L. May, L. Liu, R. Kumar, W. C. Law, H. Ding, K. T. Yong, I. Roy, M. Sheshadri, M. T. Swihart, P. N. Prasad, *Nanoscale* 2012, **4**, 5483.
20. G. J. Stasiuk, S. Tamang, D. Imbert, C. Poillot, M. Giardiello, C. Tisseyre, E. L. Barbier, P. H. Fries, M. de Waard, P. Reiss, M. Mazzanti, *ACS Nano* 2011, **5**, 8193.
21. T. Jin, Y. Yoshioka, F. Fujii, Y. Komai, J. Sekiac, A. Seiyama, *Chem. Commun.* 2008, 5764.
22. L. Prinzen, R. J. Miserus, A. Dirksen, T. M. Hackeng, N. Deckers, N. J. Bitsch, R. T. Megens, K. Douma, J. W. Heemskerk, M. E. Kooi, *et al. Nano Lett.* 2007, **7**, 93.
23. L. Liu, W. C. Law, K. T. Yong, I. Roy, H. Ding, F. Erogbogbo, X. Zhang, P. N. Prasad, *Analyst* 2011, **136**, 1881.
24. E. S. Shibu, K. Ono, S. Sugino, A. Nishioka, A. Yasuda, Y. Shigeri, S. Wakida, M. Sawada, V. Biju, *ACS Nano* 2013, **7**, 9851.
25. B. Chen, H. Zhang, C. Zhai, N. Du, C. Sun, J. Xue, D. Yang, H. Huang, B. Zhang, Q. Xie, Y. Wu, *J. Mater. Chem.* 2010, **20**, 9895.
26. H. Yang, S. Santra, G. A. Walter, P. H. Holloway, *Adv. Mater.* 2006, **18**, 2890.
27. Y. Dai, H. Xiao, J. Liu, Q. Yuan, P. Ma, D. Yang, C. Li, Z. Cheng, Z. Hou, P. Yang, J. Lin, *J. Am. Chem. Soc.* 2013, **135**, 18920.
28. T. Passuello, M. Pedroni, F. Piccinelli, S. Polizzi, P. Marzola, S. Tambalo, G. Conti, D. Benati, F. Vetrone, M. Bettinelli, A. Speghini, *Nanoscale* 2012, **4**, 7682.
29. Y. I. Park, J. H. Kim, K. T. Lee, K.-S. Jeon, H. B. Na, J. H. Yu, H. M. Kim, N. Lee, S. H. Choi, S.-I. Baik, *et al. Adv. Mater.* 2009, **21**, 4467.
30. Y. Xu, X. J. Jia, X. B. Yin, X. W. He, Y. K. Zhang, *Anal. Chem.* 2014, **86**, 12122.
31. N. Gong, H. Wang, S. Li, Y. Deng, X. Chen, L. Ye, W. Gu, *Langmuir* 2014, **30**, 10933.
32. E. S. Shibu, S. Sugino, K. Ono, H. Saito, A. Nishioka, S. Yamamura, M. Sawada, Y. Nosaka, V. Biju, *Angew. Chem. Int. Ed.* 2013, **52**, 10559.
33. X. Wu, C. Li, S. Liao, L. Li, T. Wang, Z. Su, C. Wang, J. Zhao, C. Sui, J. Lin, *Chem. Eur. J.* 2014, **20**, 8876.
34. S. K. Sun, L. X. Dong, Y. Cao, H. R. Sun, X. P. Yan, *Anal. Chem.* 2013, **85**, 8436.
35. G. Sun, L. Zhou, Y. Liub, Z. Zhao, *New J. Chem.* 2013, **37**, 1028.
36. J. Li, J. You, Y. Dai, M. Shi, C. Han, K. Xu, *Anal. Chem.* 2014, **86**, 11306.
37. J. Liu, X. Tian, N. Luo, C. Yang, J. Xiao, Y. Shao, X. Chen, G. Yang, D. Chen, L. Li, *Langmuir* 2014, **30**, 13005.
38. D. Kryza, J. Taleb, M. Janier, L. Marmuse, I. Miladi, P. Bonazza, C. Louis, P. Perriat, S. Roux, O. Tillement, C. Billotey, *Bioconjugate Chem.* 2011, **22**, 1145.
39. J. L. Bridot, A. C. Faure, S. Laurent, C. Rivière, C. Billotey, B. Hiba, M. Janier, V. Josserand, J. L. Coll, L. V. Elst, *et al. J. Am. Chem. Soc.* 2007, **129**, 5076.
40. M. Abdesselem, M. Schoeffel, I. Maurin, R. Ramodiharilafy, G. Autret, O. Clément, P. L. Tharaux, J. P. Boilot, T. Gacoin, C. Bouzigues, A. Alexandrou, *ACS Nano* 2014, **8**, 11126.
41. T. Kim, N. Lee, Y. I. Park, J. Kim, J. Kim, E. Y. Lee, M. Yi, B.-G. Kim, T. Hyeon, T. Yu, H. B. Na, *RSC Adv.* 2014, **4**, 45687.
42. K. M. Wang, X. X. He, X. H. Yang, H. Shi, *Acc. Chem. Res.* 2013, **46**, 1367.
43. M. B. Zheng, C. X. Yue, Y. F. Ma, P. Gong, P. F. Zhao, C. F. Zheng, Z. H. Sheng, P. F. Zhang, Z. H. Wang, L. T. Cai, *ACS Nano* 2013, **7**, 2056.

44. B. M. Dicheva, T. L. M. ten Hagen, L. Li, D.Schipper, A. L. B. Seynhaeve, G. C.van Rhoon, A. M. M. Eggermont, L. H. Lindner, G. A. Koning, *Nano Lett.* 2013, **13**, 2324.
45. B. R. Smith, E. E. B. Ghosn, H. Rallapalli, J. A. Prescher, T. Larson, L. A. Herzenberg, S. S. Gambhir, *Nat. Nanotechnol.* 2014, **9**, 481.
46. B. S. Kim, S. W. Park, P. T. Hammond, *ACS Nano* 2008, **2**, 386.
47. X. Zhang, C. Wang, *Chem. Soc. Rev.* 2011, **40**, 94.
48. Z. Liu, X. M. Sun, N. Nakayama-Ratchford, H. J. Dai, *ACS Nano* 2007, **1**, 50.
49. P. Horcajada, C. Serre, M. Vallet-Regi, M. Sebban, F. Taulelle, G. Ferey, *Angew. Chem. Int. Ed.* 2006, **45**, 5974.
50. V. R. Devadasu, V. Bhardwaj, M. N. V. R. Kumar, *Chem. Rev.* 2013, **113**, 1686.
51. D. Ling, W. Park, S. J. Park, Y. Lu, K. S. Kim, M. J. Hackett, B. H. Kim, H. Yim, Y. S. Jeon, K. Na, Y. Hyeon, *J. Am. Chem. Soc.* 2014, **136**, 5647.
52. V. Biju, *Chem. Soc. Rev.* 2014, **43**, 744.
53. E. S. Shibu, M. Hamada, N. Murase, V. Biju, *J. Photochem. Photobiol. C: Photochem. Rev.* 2013, **15**, 53.
54. A. Abdukayum, C. X. Yang, Q. Zhao, J. T. Chen, L. X. Dong, X. P. Yan. *Anal. Chem.* 2014, **86**, 4096.
55. H. G. Brittain, J. F. Desreux, *Inorg. Chem.* 1984, **23**, 4459.
56. F. S. Richardson, *Chem. Rev.* 1982. **82**. 541.
57. M. Li, P. R. Selvin, *J. Am. Chem. Soc.* 1995, **117**, 8132.
58. C. Quin, K. Cheng, K. Chen, X. Hu, Y. Liu, X. Lan, Y. Zhang, H. Liu, Y. Xu, L. Bu, X. Su, X. Zhu, *Sci. Rep.* 2013, **3**, 1490.
59. F. Arena, J. B. Singh, E. Gianolio, R. Stefania, S. Aime, *Bioconjugate Chem.* 2011, **22**, 2625.
60. R. D. Braun, D. Bissig, R. North, K. S. Vistisen, B. A. Berkowitz, *PLOS One* 2012, **7**, e30572.
61. G. A. F. van Tilborg, W. J. M. Mulder, N. Deckers, G. Storm, C. P. M. Reutelingsperger, G. J. Strijkers, K. Nicolay, *Bioconjugate Chem.* 2006, **17**, 741.
62. N. Kawashima, K. Nakayama, K. Itoh, T. Itoh, M. Ishiakwa, V. Biju, *Chem. Eur. J.* 2010, **16**, 1186.
63. J. Schlessinger, *Cell* 2000, **103**, 211.
64. M. Mahmoudi, H. Hofmann, B. Rothen-Rutishauser, A. Petri-Fink, *Chem. Rev.* 2012, **112**, 2323.
65. S. Sharifi, S. Behzadi, S. Laurent, M. L. Forrest, P. Stroeve, M. Mahmoudi, *Chem. Soc. Rev.* 2012, **41**, 2323.
66. L. H. Reddy, J. L. Arias, J. Nicolas, P. Couvreur, *Chem. Rev.* 2012, **112**, 5818.
67. A. Anas, H. Akita, H. Harashima, T. Itoh, M. Ishikawa, V. Biju, *J. Phys. Chem.* 2008, **112**, 10005.
68. P. Jones, S. Sugino, S. Yamamura, F. Lacy, V. Biju, *Nanoscale* 2013, **5**, 9511.
69. S. Kim, Y. T. Lim, E. G. Soltesz, A. M. De Grand, J. Lee, A. Nakayama, J. A. Parker, T. Mihaljevic, R. G. Laurence, D. M. Dor, *et al.*, *Nat. Biotechnol.* 2004, **22**, 93.
70. S. Yamashita, M. Hamada, S. Nakanishi, H. Saito, Y. Nosaka, S. Wakida, V. Biju, *Angew. Chem. Int. Ed.* 2015, **54**, 3892.
71. S. Yamashita, M. Hamada, S. Nakanishi, H. Saito, Y. Nosaka, S. Wakida, V. Biju, *Angew. Chem.* 2015, **127**, 3964.
72. E. S. Shibu, A. Sonoda, Z. Tao, Q. Feng, A. Furube, S. Masuo, L. Wang, N. Tamai, M. Ishikawa, V. Biju, *ACS Nano* 2012, **6**, 1601.
73. M. Hamada, E. S. Shibu, T. Itoh, M. S. Kiran, S. Nakanishi, M. Ishikawa, V. Biju, *Nano Reviews* 2011, **2**, 6366.
74. M. Hamada, S. Nakanishi, T. Itoh, M. Ishikawa, V. Biju, *ACS Nano* 2010, **4**, 4445.
75. V. Biju, A. Anas, H. Akita, E. S. Shibu, T. Itoh, H. Harashima, M. Ishikawa, *ACS Nano* 2012, **6**, 3776.